CROATICA CHEMICA ACTA
CCACAA **81** (3) 467–475 (2008)

ISSN-0011-1643
CCA-3266
Original Scientific Paper

Anodic Formation of Ag^I Oxide on Ag-Au Alloys*

Svetlana Grushevskaya, Dmitrii Kudryashov, and Alexander Vvedenskii**

Department of Physical Chemistry, Voronezh State University, Universitetskaya pl. 1, Voronezh, 394006, Russia

RECEIVED SEPTEMBER 27, 2006; REVISED MARCH 27, 2007; ACCEPTED JULY 24, 2007

The kinetics of anodic dissolution of silver and Ag-Au alloys (x_{Au} = 0.1–30 %) in aqueous alkaline solution under the conditions of Ag^I oxide formation has been examined. Using the techniques of cyclic voltammetry and chronoamperometry it has been established that Ag_2O anodic formation and cathodic reduction on silver and on alloys of all compositions under review are controlled by Ag^+ cation migration in the oxide layer. The oxide film consists of a thin inner layer (apparently AgOH) and of a thicker outer layer Ag_2O. These layers slightly differ in specific electro-conductivity. Using the photopotential measurements it has been shown that Ag_2O oxide is an n-type semiconductor with an excess of silver atoms. The Ag^I oxide layer formed on monocrystalline Ag(111) is more stoichiometric than the layer formed on polycrystalline Ag.

Keywords
silver
Ag-Au alloys
anodic dissolution
oxide film
photopotential

INTRODUCTION

It has been reliably established[1–12] that homogeneous binary alloys dissolve selectively. The kinetics of this process is usually investigated under the conditions of an active dissolution of the components. First of all, such situation is connected with the problem of determining partial dissolution currents, when a film of insoluble ionization products is formed. That is why the kinetics of selective dissolution (SD) of binary alloys under the conditions of salt or oxide passivation has remained practically unexamined. A possible way to solve the problem was to use Cu-Au alloys as a metallic model system.[13,14] The dissolution conditions were selected so that the electronegative component (Cu) dissolved forming an insoluble film, while the electropositive component (Au) remained thermodynamically stable in a wide potential range.

In this paper, this approach is extended to another model system – homogeneous Ag-Au alloys. Under their anodic dissolution in an alkaline medium the current registered in the polarization chain coincides with the partial current of Ag dissolution. It is important to note that the main features of SD of these alloys in the range of their active dissolution are well known[11,15–21] and the potentials of Ag^I and Ag^{II} formation noticeably differ.[22–29] The latter allowed us to carry out investigations only under the conditions of Ag_2O formation.

Thickness, porosity and structure of a passivating film can significantly influence the kinetics of selective anodic dissolution of Ag-Au alloys. In its turn, the addition of Au atoms into a silver crystal lattice must undoubtedly affect the main physicochemical properties of the film.

Since silver oxides are semiconductor structures, it is important to define the type of Ag^I oxide conductivity and deviations from the stoichiometric composition. Note that there is no single opinion even on the first issue.

---

* Part of this paper was presented at the 4th Croatian Symposium on Electrochemistry, Primošten, 2006.

** Author to whom correspondence should be addressed. (E-mail: sg@chem.vsu.ru)

Ag_2O film is considered as a p-type[30,31] or n-type[32,33] semiconductor. Important information can be derived from structure-sensitive *in situ* photoelectrochemical methods fixing the change of potential or current under UV-illumination of the oxide. In particular, a photopotential sign predetermines the type of conductivity and the amplitude determines the concentration of the prevailing structure defects.[31,34–39]

The aim of this work is to establish the main kinetic features of anodic dissolution of silver and Ag-Au alloys under the conditions of Ag^I oxide formation and to define some physicochemical and semiconductor characteristics of this oxide.

EXPERIMENTAL

Experiments were carried out on polycrystalline and monocrystalline (111) and (110) Ag-electrodes (w = 99.99 %), as well as on polycrystalline Ag-Au alloys with the gold amount fraction, x_{Au}, from 0.1 to 30 %. In addition to stationary electrodes, the rotating disc Ag-electrode (RDE) was also applied.

Polycrystalline alloys were prepared from Ag (w = 99.99 %) and gold (w = 99.99 %) at 1500 K in a vacuum quartz retort, homogenized for 72 hours at 1200 K and quenched in water. Composition of the alloys was monitored by X-ray fluorescence analysis. Single crystals were grown within two days in a horizontally moving furnace (2 mm per hour) at temperatures from 1273 K to 673 K with subsequent cooling for 24 hours. Orientation of the samples was performed using the data of X-ray diffraction analysis.

The electrode surface was mechanically polished by abrasive paper with decreasing size of grains, polished with a water-MgO suspension on suede and rinsed with doubly distilled water. Monocrystalline electrodes were mechanically polished with the water-MgO suspension and chemically polished with HCl-containing saturated chromic acid solution.

The working solution of 0.1 M KOH was prepared from doubly distilled water and reagent-grade chemicals. The solution was deoxygenated in the cell at 298 K by passing chemically pure argon. A counter Pt electrode, Ag, AgCl/Cl reference electrode with a Luggin capillary and salt bridge were used. All potentials are referred to the standard hydrogen electrode scale.

Before starting the experiments, the state of the electrode surface was electrochemically standardized by 5-min cathodic prepolarization at E_s = –0.4 V. In cyclic i-$E(t)$ measurements the electrode potential was scanned from E_s to E_f and back at the rate of v = 1–80 mV s^{-1}. In some experiments, after the first anodic-cathodic polarization cycle, the electrode was not extracted from the solution to immediately undergo the second and third cycles under the same regime. The current transients were registered for 1800 s by switching the potential from E_s to experimental value E. The current densities are referred to the unit of electrode geometric surface S_g (0.3–0.8 cm^2).

Ag^I oxide for photoelectrochemical measurements was formed potentiostatically at E = 0.48–0.52 V on stationary Ag-electrodes. The photopotential V_{ph} measurements were carried out 20 s after switching off the anodic polarization. V_{ph}-t dependences were recorded with the aid of DAC + PC. To estimate the possible contribution of surface electronic states connected with reagents adsorption, the active and reactive impedance components of silver-solution interface were determined before and after the experiments. Thickness L of the film was determined coulometrically from the charge required to reduce the oxide film.

A set of light-emitting diodes was used for UV-illumination. A wide spectrum of wavelengths of diodes (λ = 385–875 nm) makes it possible to change discretely the energy of light quantum in the range of 1.4–3.2 eV. The duration of illumination pulse was 2 ms, the repetition frequency was 5 Hz. The ratio of dark and light periods was 0.01, which excluded the influence of the previous pulse on photo-signal parameters. In all experiments, the power of light pulse was monitored and could be varied from 0.75 to 3 mW cm^{-2}. The use of a low-noise amplifier, an active filter of fifth-order frequency and digital signal processing made it possible to reduce the noise level to 1–2 μV.

RESULTS AND DISCUSSION

Cyclic Voltammetry of Silver

Shape of the i-$E(t)$ curve on a stationary Ag-electrode at $E_f \leq 0.65$ V is typical only of Ag^I oxide formation and its subsequent reduction (Figure 1). This process is described by the following overall reaction:[23–29]

$$2\ Ag + 2\ OH^- = Ag_2O + H_2O + 2\ e^- \qquad (1)$$

where the equilibrium potential at 298 K is:

$$E_{Ag_2O/OH^-} = 0.345 - 0.059\ \log(a_{OH^-} / a_{Ag}) \qquad (2)$$

In an aqueous solution with c_{OH^-} = 0.1 mol dm^{-3}, the value of E_{Ag_2O/OH^-} is 0.409 V at a_{Ag} = 1. Hence it can be assumed that the anodic (A) and cathodic (C) peaks correspond to the processes of Ag^I oxide formation and reduction proceeding with a noticeable overpotential.

To define the nature of overpotential, the experiments with different scan rates v and different rotating rates of Ag-RDE were conducted. It was revealed that the growth of v practically does not change the shape of cyclic voltamograms but it causes a significant enhancement of anodic i_A and cathodic i_C maximal currents, as well as a shift of anodic E_A and cathodic E_C peak potentials to more positive and more negative values, respectively. Linear dependence of i_A and i_C on $v^{1/2}$ (Figure 2) points[40] to the appearance of diffusion limitation in Ag^I oxide formation and reduction. Taking into account the lack of noticeable influence of the RDE rotating rate on the shape of voltamograms and peak currents, we con-

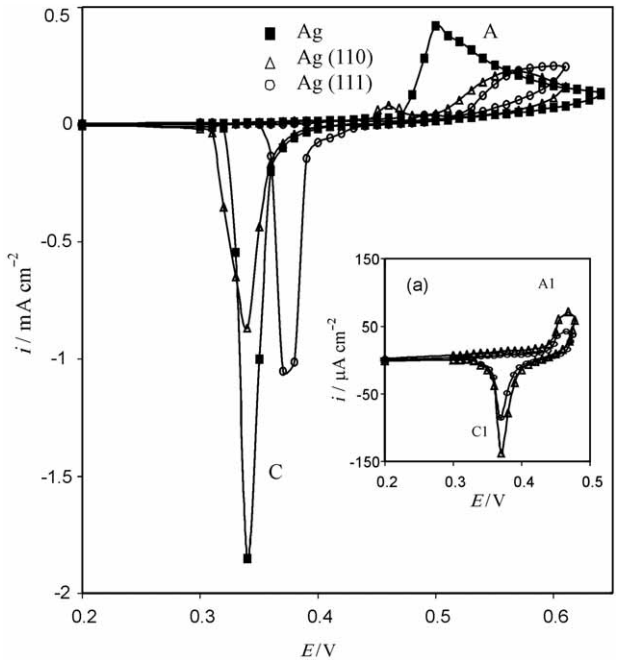

Figure 1. Cyclic voltamograms of polycrystalline and monocrystalline Ag in 0.1 M KOH at $v = 1$ mV s^{-1}.

clude that the solid phase mass transport in the oxide film is the rate-controlling stage after the oxide phase has been formed. The same kinetics was established earlier.[23,24,28,29] The stage of nucleation is apparently very fast; hence it is not revealed by voltammetric measurements.

The shape of cyclic voltamograms changes in transition from polycrystalline to monocrystalline Ag-electrodes (Figure 1). The peak of oxide formation A becomes less clear-cut and shifts to positive values almost by 60 mV (the potential E_A reaches 0.56–0.58 V for Ag(111),[41] which is in good agreement with our data); peak current i_A decreases approximately two times. Thus, Ag^I oxide formation on monocrystalline electrodes is slightly hampered.

At the same time the anodic prepeak A1 at potential of about 0.46 V is revealed on monocrystalline electrodes more clearly than on polycrystalline Ag. The short voltamograms of Ag(111) and Ag(110) show also the cathodic maximum C1 corresponding to the anodic prepeak A1 (Figure 1a). The anodic charge at the moment of reaching E_{A1} reflects the formation of at least some monolayers of Ag^I oxide. In our opinion, these facts prove the phase but not the adsorption nature of the product formed in the range of prepeak A1. In the long cycle, prepeak C1 is not revealed, being overlapped by the reduction peak C of the main product Ag_2O.

Note that the nature of the prepeak on the anodic voltamogram of silver in alkaline solutions was repeatedly discussed earlier.[25,28,29,41–43] As a rule, its appearance is considered to be connected with the formation of one or more monolayers of AgOH or Ag_2O before the formation of the bulk Ag_2O layer. Using the obtained data and taking into account the results of numerous papers, we assume that the oxide film at the Ag-electrode surface has a duplex structure. The following sequence of reactions is possible at the initial stage of Ag^I oxide anodic formation:

$$Ag + OH^- = AgOH^- (ad) \quad (3)$$

$$AgOH^-(ad) = AgOH(ad) + e^- \quad (4)$$

$$2\ AgOH(ad) = Ag_2O + H_2O \quad (5)$$

Reaction (5) combines stages of 2D- and/or 3D-nucleation, growth of nuclei of over-critical size and the formation of Ag^I oxide phase layer. It is not improbable that the initial phase product is Ag^I hydroxide and the oxide arises in the course of the following phase transformation:

$$AgOH(ad) = AgOH \quad (6)$$

$$2\ AgOH = Ag_2O + H_2O \quad (7)$$

In this case, the film of Ag^I hydroxide with a thickness of several monolayers is formed at the potential of prepeak A1. A more disordered Ag_2O layer grows above the inner hydroxide (peak A). (Note that these schemes do not take into account silver dissolution with the formation of hydroxyl-complexes, such as $Ag(OH)_2^-$, or more complicated ones, nor the possible AgOH and Ag_2O dissolution.)

Cyclic Voltammetry of Ag-Au Alloys

Kinetic investigations of SD of alloys are complicated by the appearance of an additional possible rate-controlling factor. Selective dissolution is usually accompanied by the formation of a surface layer depleted by an electronegative component. It is therefore necessary to take into account a solid-phase flux of atoms in this layer from the alloy volume to the surface. In this case:

$$Ag_{(v)} \rightarrow Ag_{(s)} \quad (8)$$

It is stage (8) that limits the SD of Ag-Au alloys at the potentials of active dissolution.[11] If the phase film of oxidation product is formed at the alloy surface, then the question arises – which solid phase (alloy or oxide) causes the transport limitation? To establish the nature of the phase, in which the mass transport defining the rate of oxide formation and reduction on alloys is localized, the diagnostic criteria based on the theory of cyclic voltammetry[42] were elaborated:[13,14]

$$\frac{i_A(\text{alloy})}{i_A(\text{Ag})} = \begin{cases} \dfrac{(D_{Ag})^{1/2}}{(D_{Ag^+})^{1/2}} & \text{(mass transport in alloy)} \\ \dfrac{(D_{Ag^+}{}^*)^{1/2}}{(D_{Ag^+})^{1/2}} & \text{(mass transport in film)} \end{cases} \quad (9)$$

$$E_A(\text{alloy}) - E_A(\text{Ag}) = [E_{Ag_2O\,/\,OH^-}(\text{alloy}) - E_{Ag_2O\,/\,OH^-}(\text{Ag})] + + \begin{cases} \dfrac{1}{2}\times\dfrac{2.3RT}{F}\lg\dfrac{D_{Ag^+}}{D_{Ag}} & \text{(mass transport in alloy)} \\ \dfrac{1}{2}\times\dfrac{2.3RT}{F}\lg\dfrac{D_{Ag^+}}{D_{Ag^+}{}^*} & \text{(mass transport in film)} \end{cases} \quad (10)$$

Here, D_{Ag}, D_{Ag^+} and $D_{Ag^+}{}^*$ are diffusion coefficients of Ag atoms in the alloy and of Ag^+ ions in the oxide grown on silver and the Ag-Au alloy, respectively. For non-polarized Ag-Au alloys with the predominance of silver, the equilibrium potentials of oxide formation E_{Ag_2O/OH^-} (alloy) slightly differ from E_{Ag_2O/OH^-} (Ag). If, in addition, $D_{Ag} << D_{Ag^+}$ and D_{Ag^+} is close to $D_{Ag^+}{}^*$, then the following conditions are valid for a limiting mass transport in the alloy:

$$E_A(\text{alloy}) - E_A(\text{Ag}) >> 0.030\ \text{V} \quad (11a)$$

$$i_A(\text{alloy}) \,/\, i_A(\text{Ag}) << 1 \quad (11b)$$

When the process of SD is limited by mass transport in the film, then under the same conditions:

$$E_A(\text{alloy}) - E_A(\text{Ag}) \approx 0 \quad (12a)$$

$$i_A(\text{alloy}) \,/\, i_A(\text{Ag}) \approx 1 \quad (12b)$$

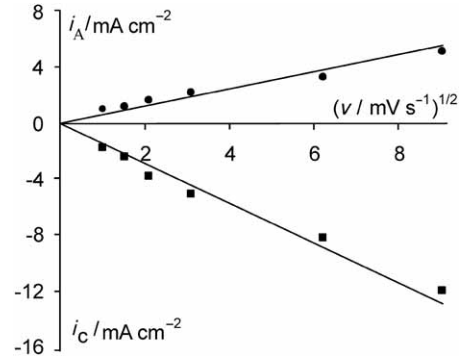

Figure 2. Dependence of maximal anodic and cathodic currents on the scan rate for polycrystalline Ag in 0.1 mol dm^{-3} KOH.

Application of criteria (11a) and (12a) is complicated if the active SD period precedes the oxide formation. In this case, E_{Ag_2O/OH^-} (alloy) and E_{Ag_2O/OH^-} (Ag) can be significantly different, since in (2) now appears not a volume but a surface silver activity ($a_{Ag}{}^s = \gamma_{Ag}{}^s \cdot x_{Ag}{}^s$). Note that in the course of SD the surface silver concentration can decrease noticeably compared to volume concentration; therefore one cannot neglect the first term in (10).

Equations (9) and (10), as well as (11) and (12) following them can also be applied to the cathodic process of oxide reduction accompanied by silver diffusion into the bulk Ag-Au alloy. But the currents and the potentials of cathodic peaks (i_C and E_C) must be used in Eqs. (9) to (12).

The experimental data show that the potential E_C of Ag_2O reduction remains practically constant for Ag and alloys of all compositions regardless of the scan cycle. The difference between E_C(alloy) and E_C(Ag) does not exceed 0.02 V. The ratio i_C(alloy) / i_C(Ag) slightly and non-systematically changes (Table I). This means, in ac-

TABLE I. Parameters of cyclic voltammetry of Ag_2O formation and reduction on Ag-Au alloys

Parameter	Cycle	x(Au) / %					
		0.1	0.3	1	4	15	30
$(E_C(\text{alloy}) - E_C(\text{Ag}))$ / V	I	0	0.010	0.010	0.010	0.010	0.020
	II	0	0.010	0.010	0.010	0.010	0.020
	III	0	0.010	0.010	0.010	0.010	0.020
$(E_A(\text{alloy}) - E_A(\text{Ag}))$ / V	I	0.015	0.015	0.015	0.015	0.225	–
	II	0	0	0	0	0.010	0.020
	III	0	0	0	0	0	0.020
i_C (alloy) / i_C (Ag)	I	0.60	0.80	0.81	0.80	1.02	0.41
	II	0.70	0.81	0.83	0.78	0.92	0.41
	III	0.68	0.80	0.81	0.74	0.95	0.45
i_A (alloy) / i_A (Ag)	I	0.50	0.38	0.52	0.58	1.38	–
	II	0.48	0.34	0.43	0.42	0.40	0.12
	III	0.52	0.38	0.46	0.42	0.47	0.16

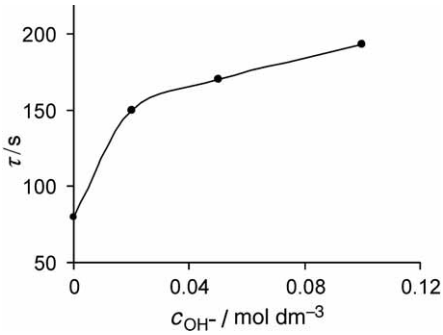

Figure 3. Influence of c_{OH^-} on the transition time of Ag_2O galvanostatic reduction in x mol dm^{-3} KOH + (0.2 – x) mol dm^{-3} KNO_3.

cordance with criteria (12a) and (12b), that the cathodic reduction of oxide film on silver and Ag-Au alloys is limited by mass transport in the oxide phase. Besides, we can assume that the mobility of diffusate (presumably Ag^+ cation) in the Ag_2O film formed on Ag and Ag-Au alloys is practically of the same value.

In a separate set of galvanostatic experiments on Ag_2O reduction in solutions with constant ionic force, it was shown that the transition time τ of the oxide reduction significantly grows with an increase in OH^--ions concentration (Figure 3). In this case,[44] the mass transport in the film is mainly realized by Ag^+-cations. In the case of anion mass transport, τ does not depend on the anion concentration in the solution.

Let us turn our attention to the parameters of Ag^I oxide formation. It has been established that up to the amount fraction of gold in the alloy, $x_{Au} \leq 4$ %, the difference E_A(alloy) – E_A(Ag) does not exceed 15 mV (Table I). The ratio i_A(alloy) / i_A(Ag) insignificantly and non-systematically changes with x_{Au}; anodic peak currents on the alloys are, as a rule, slightly lower than on silver. Following the criteria (12a) and (12b), we conclude that in the low-concentrated alloys based on silver the mass transport in the Ag^I oxide film is the rate-controlling stage of anodic dissolution, as it is for silver.

On the voltamogram of Ag-15Au alloy, the peak of Ag_2O formation in the first polarization cycle is shifted by 0.225 V to positive values but the ratio i_A(alloy) / i_A(Ag) remains close to unity. This peak is not revealed for the Ag-30Au alloy in spite of the increase of E_f to the range of oxygen release (Figure 4). Nevertheless, a certain quantity of Ag_2O and, probably, of AgO (peak A2) appears, causing the corresponding cathodic peaks.

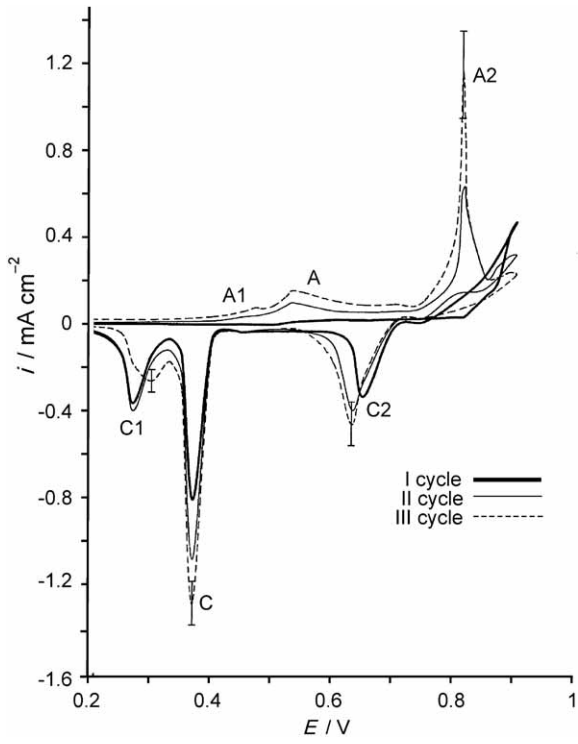

Figure 4. Multi-cyclic voltamogram of Ag-30Au alloy in 0.1 M KOH at v = 1 mV s^{-1}.

The data obtained can be explained if one assumes that in the alloys with $x_{Au} \geq 15$ % the period of active SD of Ag precedes the formation of Ag^I oxide. Since the observed difference between E_A(alloy) and E_A(Ag) is now caused not by the second term in (10) but by the first one, the main criteria for kinetics definition are (11b) and (12b). On the whole, we conclude that the anodic formation of Ag^I oxide on Ag-Au alloys of all compositions under review is limited by mass transport in the oxide film.

The results of the second and following cycles of anodic-cathodic polarization of alloys are very illustrative. The alloy surface is now covered with micro-disperse silver, where the formation of Ag_2O and then of AgO takes place. Therefore the potential of Ag^I oxide formation at cycles of polarization II and III is about 0.50–0.52 V and practically does not change with gold content in the alloy. The current ratio i_A(alloy) / i_A(Ag) is close to unity. The absolute values of current i_A in polarization cycle I are lower than in cycles II and III. The

TABLE II. The capacity of Ag-electrode, peak current and full charge at the end of polarization cycles I, II and III

Cycle number, i	C^i / C^{i-1}	$I_A{}^i$ / $I_A{}^{i-1}$	$I_C{}^i$ / $I_C{}^{i-1}$	$Q_a{}^i$ / $Q_a{}^{i-1}$	$Q_c{}^i$ / $Q_c{}^{i-1}$
II	1.47	1.50	1.40	1.43	1.45
III	1.17	1.11	1.13	1.14	1.15

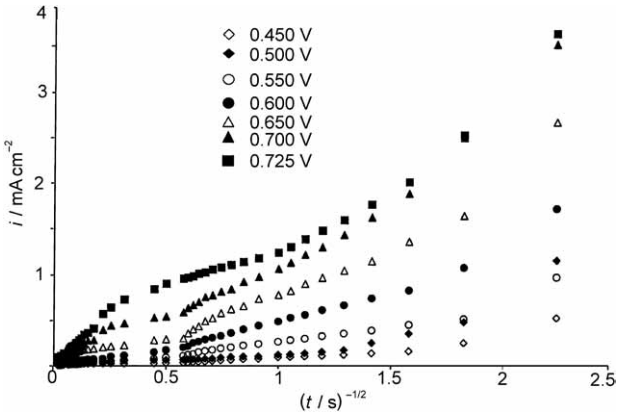

Figure 5. Current transients of Ag-15Au alloy in 0.1 mol dm^{-3} KOH.

latter is connected with the growth of the electrode surface roughness factor obtained by the data of capacity measurements before and after each polarization cycle (Table II).

The ratio of capacity after each polarization cycle (C^i) to the capacity after the previous polarization cycle (C^{i-1}) coincides with the relevant ratio of currents in anodic I_A and cathodic I_C peaks of voltamograms (Table II). The same is valid for the charges passed during the anodic Q_a and cathodic Q_c periods of *i-E* curves recording.

Chronoammetry of Silver and Ag-Au Alloys

Anodic current transients for silver and its alloys with gold in the potential range of Ag_2O formation are of the same shape. Lack of a typical nucleation maximum shows that i) the oxide formation current is masked by more significant currents of silver dissolution with the formation of hydroxyl-complexes or ii) the phase layer of Ag^I oxide has been already formed by the beginning of *i-t* curves registration ($t \geq 0.5$ s). The shape of current transients for silver and Ag-Au alloys in Cottrel coordinates (being indicative of volume diffusion) is rather complicated (Figure 5). As a rule, 2–3 linear plots with sharp slopes and the range of relative current stabilization over longer periods are revealed. On all the plots of

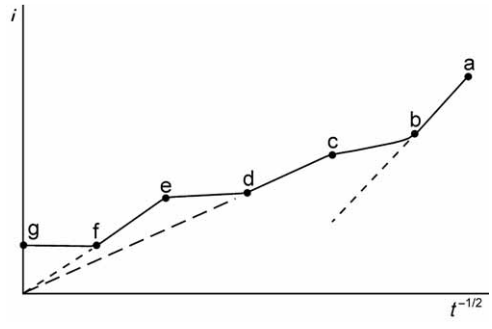

Figure 6. Scheme of current transients for Ag_2O formation on Ag and Ag-Au alloys in 0.1 M KOH.

i-t curves, the current significantly grows as the anodic potential of Ag^I oxide formation increases. The latter makes it possible to consider mass transport mainly as a migration process.

Figure 6 shows a full scheme of typical current transients in $i\text{-}t^{-1/2}$ coordinates. It contains three linear plots (a-b, c-d, e-f), two transition ranges (b-c, d-e) and a range of current stabilization (f-g). At low enough values of the anodic potential, only a part of a full curve restricted by range d-e is observed. At mean values, registration of a full curve is possible. But at high values, the processes corresponding to plots a-b and b-c apparently come to an end by the beginning of the *i-t* curve registration.

The analysis of chronocoulograms obtained by integration of *i-t* curves shows that regardless of the electrode nature, the formation of oxide film with an effective thickness of no more than 3–4 atomic layers (with due account of the roughness factor, this layer is even thinner) corresponds to the plot a-b. Such a film cannot physically be a zone of non-stationary mass transport. Most probably, the adsorption and nucleation processes of the initial oxide formation proceed in these periods of time. (Note that the complex shape of $i\text{-}t^{-1/2}$ dependences was also registered during the anodic formation of Ag_2O at $t < 1$ s,[45] which was explained by the possible influence of nucleation processes.) The plot c-d is apparently connected with the formation of a compact inner anodic film (Ag_2O or AgOH) with a thickness of some monolayers. At the plot e-f, the formation of the general outer film Ag_2O with a thickness of more than 20 monolayers probably takes place. Using the film thickness data as the criterion and model of the duplex structure of Ag^I oxide film, we sorted linear plots of experimental $i\text{-}t^{-1/2}$ curve groups as belonging either to the range c-d (AgOH formation) or the range e-f (Ag_2O formation). Further quantitative processing of these plots was carried out by a model of non-stationary migration in a thickening film of constant porosity:[46]

$$i(t) = \left[\frac{zF\sigma\rho\eta}{M}\right]^{1/2} \frac{1}{t^{1/2}} = \frac{K}{t^{1/2}} \qquad (13)$$

Here, ρ is the density of Ag_2O, M is the molecular weight of Ag_2O, σ is specific conductivity of Ag_2O, $\eta = E - E_{Ag_2O/OH^-}$ is the overpotential of oxide formation and K is the effective constant of mass transport. The applicability of this model is proved not only by current transients linearization in $i\text{-}t^{-1/2}$ coordinates, but also by the appearance of linear plots $K\text{-}\eta^{1/2}$ for different electrodes at t = const. (Figure 7).

It has been revealed that the mean values of σ_{AgOH} and σ_{Ag_2O} obtained from $i\text{-}t^{-1/2}$ dependence slope at different stages of the oxide film formation on silver in one and the same potential range $E < 0.525$ V practically do not differ ($1.03 \times 10^{-6}\ \Omega^{-1}\ m^{-1}$ and $1.48 \times 10^{-6}\ \Omega^{-1}\ m^{-1}$). Note that the specific conductivity of Ag_2O extracted

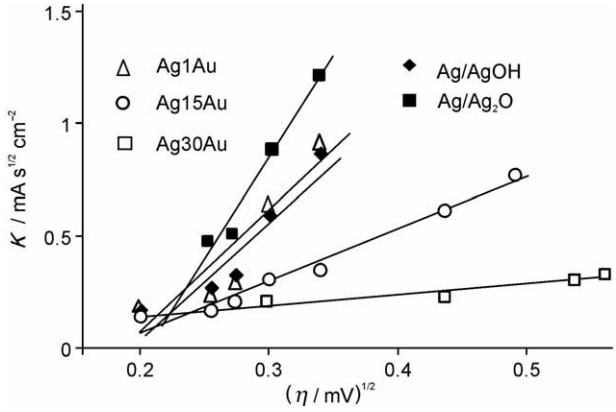

Figure 7. Overpotential dependence of the effective constant of mass transport in the processes of oxide formation on Ag and Ag-Au alloys in 0.1 mol dm^{-3} KOH.

from the solution and dried is 1.0×10^{-6} Ω^{-1} m^{-1} (Ref. 23) or 1.25×10^{-5} Ω^{-1} m^{-1}.[27]

For the Ag-1Au alloy, plots c-d and e-f practically overlap; hence the overall value $\sigma_{Ag_2O} \approx 2.32 \times 10^{-6}$ Ω^{-1} m^{-1} was estimated. For alloys with a high concentration of gold, the calculated data of σ appears to be one or two orders lower, which is extremely improbable from the physical point of view. In fact, under the prevailing migration of the Ag^+ cation in the oxide the following equation holds: $\sigma \approx F^2 c_{Ag^+} D_{Ag^+} / RT$. The values of D_{Ag^+} practically do not change in transition from silver to Ag-Au alloys. Most probably, the concentration of the main charge carriers (c_{Ag^+}) remains unchanged as well. These facts allow us to assume that the sharp decay in specific conductivity of Ag^{I} oxide grown on Ag-Au alloys is illusive. The cause lies in equation (13), which needs a certain value of η for σ definition. But, η can be sufficiently decreased if the potential E_{Ag_2O/OH^-} (alloy) is shifted to positive values because of an active SD of silver at the initial stage of the oxide formation (discussed above). Unfortunately, all quantitative estimations of σ are out of the question in this case.

All the data presented allow us to conclude that the formation as well as the reduction of Ag^{I} oxide on silver and Ag-Au alloys are controlled by Ag^+ migration in the oxide film. An analogous conclusion was made earlier for the anodic dissolution of Cu-Au alloys with $x_{Au} \leq 30$ % under the conditions of Cu_2O formation.[13,14] The peculiarity of Ag-Au system is connected with the presence of an initial stage of active SD of silver from Ag-15Au and Ag-30Au alloys preceding the oxide formation. In Cu-Au alloys of the same composition, this stage is not revealed in kinetic measurements.

Photopotential Measurements

Regardless of the conditions of Ag_2O film formation on silver and of the parameters of UV-illumination (intensity, wave length), the values of V_{ph} are negative. This points to the n-type of conductivity in crystalline oxide and to the predominance of donor defects in its structure.[31,34–39] Oxygen vacancies or superstoichiometric silver atoms can play the role of such defects. Taking into account the cation character of silver oxidation, one should consider the appearance of superstoichiometric Ag atoms in the Ag_2O structure, which confirms the assumption about Ag^+ ions as the main charge carriers in the film.

The photopotential gradually decreases with time, achieving the stationary level at $t \approx 600$ s. This decay is caused by self-dissolution of the film, as it was shown in special experiments. The dependence $\ln(V_{ph})$-t is linear (Figure 8), which allows us to determine the initial value of photopotential $V_{ph}(0)$ by extrapolating the graph to $t \rightarrow 0$.

$V_{ph}(0)$ practically does not depend on the film formation potential, but it significantly increases with the density of anodic charge q, *i.e.,* with thickness L of the oxide layer (Table III).

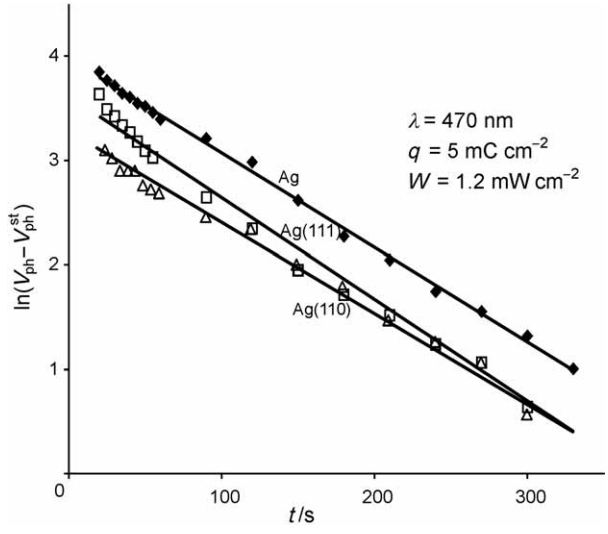

Figure 8. Photopotential decay in Ag_2O film after switching off Ag polarization in 0.1 M KOH.

TABLE III. Initial values of photopotential $V_{ph}(0)$ in Ag_2O formed on polycrystalline Ag at $\lambda = 470$ nm and $W = 1.2$ mW cm^{-2}

L / nm	$V_{ph}(0)$ / μV		
	E = 0.485 V	E = 0.495 V	E = 0.505 V
6.4	–13	–15	–10
9.6	–17	–29	–24
12.8	–29	–35	–28
16.0	–56	–58	–61
22.4	–104	–114	–146

[a] L, oxide layer thickness; E, film formation potential.

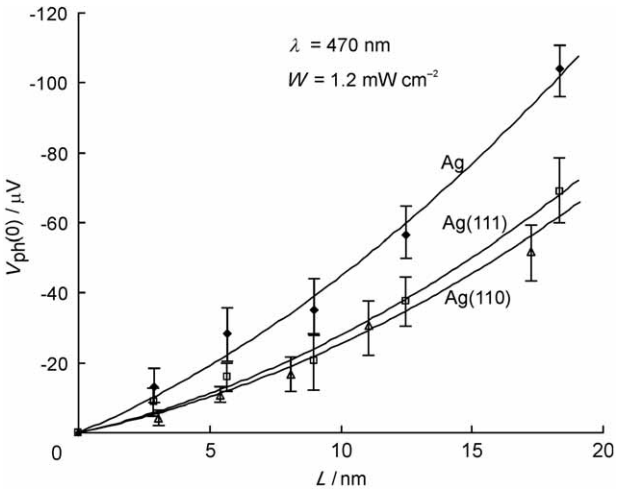

Figure 9. Dependence of photopotential on the Ag_2O film thickness.

The appearance of $V_{ph}(0)$-L dependence (Figure 9) allows us to consider the anodic film as a »thin« film with Debye's range $l_D >> L$.[39] In this case, the photopotential can be represented (with some assumptions) as follows:

$$V_{ph}(0) \approx -\frac{edLN_D}{\varepsilon\varepsilon_0} \qquad (14)$$

where d = 0.472 nm is the Ag_2O lattice constant; $\varepsilon(Ag_2O)$ = 8.8;[47] N_D is the volume concentration of donor defects. The latter, calculated from the initial slope of V_{ph}-L dependence, is 4.3×10^{16} cm^{-3}.

All the features mentioned above are valid for the photopotential of the oxide layer formed on monocrystalline Ag(111) and Ag(110). But, the V_{ph} amplitude is noticeably lower (Figure 8), which proves the formation of Ag_2O oxide with a more ordered structure. In this case, the concentration of super-stoichiometric silver atoms decreases to 1.6×10^{16} cm^{-3} for Ag(111) and 1.3×10^{16} cm^{-3} for Ag(110).

CONCLUSIONS

– Anodic dissolution of Ag and Ag-Au alloys, x_{Au} = 0.1–30 %, in alkaline solution under the conditions of Ag_2O formation is controlled by the migration of Ag^+ ions *via* the oxide film. For Ag-15Au and Ag-30Au alloys, the appearance of a short initial stage of active SD of silver preceding the oxide growth is assumed.

– Cathodic reduction of Ag_2O is also limited by mass transport in the oxide phase. Mobility of Ag^+ cations in Ag_2O films obtained on silver and Ag-Au alloys is the same. Chemical composition of alloys practically does not influence the parameters of Ag^I oxide reduction.

– Ag_2O film has a duplex structure. For the Ag-electrode, a thin inner layer (apparently AgOH) and a thicker outer layer slightly differ in specific electroconductivity ($(1.0–1.5) \times 10^{-6}$ Ω^{-1} m^{-1}).

– Ag_2O oxide is an n-type semiconductor with an excess of silver atoms in the lattice regardless of the potential of film formation. On monocrystalline Ag(111) and Ag(110), as opposed to polycrystalline silver, a more stoichiometric Ag^I oxide is formed.

Acknowledgements. – This work is supported by the Ministry of Education and Science of the Russian Federation (project RNP 2.2.2.3.3128), CRDF (grant RUXO-000010-VZ-06) and RFBR (project 06-03-32274-a).

REFERENCES

1. H. Kaiser and H. Kaesche, *Werkst. Korros.* **31** (1980) 347–353.
2. H. Kaiser, *Alloy Dissolution, Chemical Industries,* V. 28, Marcel Dekker, New York, Basel, 1987, pp. 85–118.
3. A. J. Forty and G. Rowlands, *Philos. Mag.* **43A** (1981) 171–188.
4. S. Rambert and D. Landolt, *Electrochim. Acta* **31** (1986) 1433–1441.
5. M. Seo, *Boshoku Gijutsu. Corros. Eng.* **33** (1984) 162–169.
6. H. W. Pickering, *Corros. Sci.* **23** (1983) 1107–1120.
7. M. J. Pryor and J. C. Fister, *J. Electrochem. Soc*. **131** (1984) 1230–1235.
8. K. Sieradski, R. R. Corderman, K. Shukla, and R. C. Newman, *Philos. Mag.* **59** (1989) 713–746.
9. J. J. Gardiazabal and J. R. Galvele, *J. Electrochem. Soc*. **127** (1980) 255–258.
10. Ya. M. Kolotyrkin, *Zaschita Metallov* **19** (1983) 675–683.
11. I. K. Marshakov, A. V. Vvedenskii, V. Yu. Kondrashin, and G. A. Bokov, *Anodnoe Rastvorenie i Selektivnaya Korrosiya Splavov*, VSU, Voronezh, 1988, p. 402.
12. V. V. Losev and A. P. Pchel'nikov, *Itogi Nauki i Tekhniki: Electrokhimiya* **15** (1979) 62–131.
13. S. N. Grushevskaya and A. V. Vvedenskii, *Zaschita Metallov* **35** (1999) 346–354.
14. A. V. Vvedenskii and S. N. Grushevskaya, *Corros. Sci.* **45** (2003) 2391–2413.
15. H. W. Pickering and C. Wagner, *J. Electrochem. Soc.* **114** (1967) 698–706.
16. H. W. Pickering, *J. Electrochem. Soc.* **115** (1968) 143–147.
17. F. Lantelme and S. Belaidonni, *Electrochim. Acta* **26** (1981) 1225–1236.
18. G. Hultguist and H. Hero, *Corros. Sci.* **24** (1984) 789–805.
19. B. W. Parks, J. D. Fritz, and H. W. Pickering, *Scripta Met.* **23** (1989) 951–956.
20. A. V. Vvedenskii, I. K. Marshakov, and V. N. Storozhenko, *Electrokhimiya* **30** (1994) 459–472.
21. A. V. Vvedenskii and I. K. Marshakov, *Electrokhimiya* **33** (1997) 298–307.
22. T. A. Kuznetsova, E. V. Flegel, and A. V. Vvedenskii, *Zaschita Metallov* **38** (2002) 379–386.

23. N. A. Hampson, J. B. Lee, and J. R. Morley, *Electrochim. Acta* **16** (1971) 637–642.
24. T. G. Clarke, N. A. Hampson, J. B. Lee, J. R. Morley, and B. Scanlon, *Ber. Bunsenges. Phys. Chem.* **73** (1969) 279–283.
25. M. L. Teijelo, J. R. Vilche, and A. J. Arvia, *J. Electroanal. Chem.* **162** (1984) 207–224.
26. P. Stonehart, *Electrochim. Acta* **13** (1968) 1789–1803.
27. M. J. Dignam, H. M. Barret, and G. D. Nagy, *Can. J. Chem*. **47** (1969) 4253–4266.
28. B. V. Tilak, R. S. Perkins, H. A. Kozlovska, and B. E. Convay, *Electrochim. Acta* **17** (1972) 1447–1469.
29. J. Ambrose and R. G. Barradas, *Electrochim. Acta* **19** (1974) 781–786.
30. D. Ross and E. F. I. Roberts, *Electrochim. Acta* **21** (1976) 371–375.
31. E. K. Oshe and I. L. Rosenfeld, *Zaschita Metallov* **5** (1969) 524–531.
32. Z. Jiang, S. Huang, and B. Qian, *Electrochim. Acta* **39** (1994) 2465–2470.
33. R. S. Perkins, B. V. Tilak, B. E. Convay, and H. A. Kozlovska, *Electrochim. Acta* **17** (1972)1471–1489.
34. Yu. Ya. Gurevich and Yu. V. Pleskov, *Fotoelectrokhimia Poluprovodnikov*, Nauka, Moscow, 1983, p. 312.
35. H. O. Finklea, *Semiconductor Electrodes*, Elsevier, Amsterdam-Oxford-New York-Tokyo, 1988, p. 519.
36. J. O'M. Bockris and S. U. M. Khan, *Surface Electrochemistry,* Plenum Press, New York, London, 2004, p. 354.
37. E. K. Oshe and I. L. Rosenfeld, *Itogi Nauki i Techniki: Korrozia i Zaschita ot Korrozii* **7** (1978) 111–158.
38. F. F. Volkenshtein and V. V. Malahov, *Zhurnal Fizicheskoi Khimii* **69** (1975) 3157–3160.
39. F. F. Volkenshtein and V. V. Malahov, *Zhurnal Fizicheskoi Khimii* **69** (1975) 3161–3164.
40. Z. Galus, *Teoretyczne podstawy electroanalizy chemiczney*, Panstwowe Wydawnictvo Naukove, Warszawa, 1971, p. 552.
41. J. Kunze, H.-H. Strehblow, and G. Staikov, *Electrochem. Commun.* **6** (2004) 132–137.
42. C. Alonso, R. C. Salvarezza, J. M. Vara, and A. J. Arvia, *Electrochim. Acta* **35** (1990) 489–496.
43. J. Gomez Becerra, R. C.Salvarezza, and A. J. Arvia, *Electrochim. Acta* **35** (1990) 595–604.
44. K. S. Cemezova, N. M. Hlynova, and O. S. Ageeva, *Elektrokhimia* **36** (2000) 763–766.
45. B. M. Jovic and V. D. Jovic, *J. Serb. Chem. Soc*. **69** (2004) 153–166.
46. V. I. Birss and G. A. Wright, *Electrochim. Acta* **26** (1981) 1809–1817.
47. B. P. Nikol'skii (Ed.), *Spravochnik khimika,* V. 1, Khimiya, Leningrad, p. 1072.

SAŽETAK

Anodno nastajanje Ag^I oksida na Ag-Au legurama

Svetlana Grushevskaya, Dmitrii Kudryashov i Alexander Vvedenskii

Ispitivana je kinetika anodnog otapanja srebra i Ag-Au legura (x_{Au} = 0,1–30 %) u lužnatim otopinama u uvjetima stvaranja Ag^I oksida. Primjenom cikličke voltametrije i kronoamperometrije ustanovljeno je da anodno nastajanje Ag_2O i katodnu redukciju na srebru i legurama svih ispitivanih sastava kontrolira migracija Ag^+ kationa u oksidni sloj. Oksidni film sastoji se od tankog unutarnjeg sloja (očito AgOH) i od debljeg vanjskog sloja Ag_2O. Ovi se slojevi ponešto razlikuju po specifičnoj električnoj vodljivosti. Metodom mjerenja fotopotencijala pokazano je da je oksid Ag_2O poluvodič n-tipa s viškom atoma srebra. Oksidni sloj Ag^I, koji se formira na Ag(111) monokristalu, bliži je stehiometrijskom sastavu od oksidnog sloja formiranog na polikristaliničnom Ag.